PCCP

ROYAL SOCIETY OF CHEMISTRY

COMMUNICATION

View Article Online
View Journal | View Issue

Cite this: *Phys. Chem. Chem. Phys.*, 2025, **27**, 21867

Received 30th August 2025,
Accepted 27th September 2025

DOI: 10.1039/d5cp03335g

rsc.li/pccp

Electric field-induced circularly polarised luminescence switching in chiral nematic liquid crystals with negative dielectric anisotropy

Daiya Suzuki,[a] Kosuke Kaneko [b] and Yoshitane Imai *[a]

An emissive chiral nematic liquid crystal (*N-LC-MBBA/CPDI) was fabricated by doping an achiral nematic liquid crystal (*N*-LC), namely *N*-(4-methoxybenzylidene)-4-butylaniline (MBBA), which exhibits a negative dielectric anisotropy ($\Delta\varepsilon < 0$), with the chiral luminophore *N*,*N*′-bis(1-cyclohexylethyl)perylene-3,4,9,10-tetracarboxylic diimide (CPDI). In contrast to the previously reported emissive chiral *N*-LC (*N**-LC-6CB/CPDI) composed of a positive dielectric anisotropy *N*-LC, *N**-LC-MBBA/CPDI exhibited no circularly polarised luminescence (CPL) in the absence of a direct current (DC) electric field. However, upon the application of a DC electric field, a pronounced CPL signal emerged due to helical axis reorientation in the chiral nematic host. Under the optimised conditions, the system displayed a high dissymmetry factor with $|g_{CPL}|$ values reaching up to 0.36. Moreover, the CPL response was reversible and continuously switchable upon electric field modulation. Overall, this study presents an effective strategy for the development of functional CPL-switching devices based on the DC field-driven control of *N**-LCs.**

Chiral nematic liquid crystals (*N**-LCs), which are formed by doping nematic liquid crystals (*N*-LCs) with a small amount of chiral dopants, exhibit characteristic helical structures that impart unique optical properties, including circularly polarised luminescence (CPL).[1–5] The dynamic control of these helical structures by external stimuli has attracted significant attention in recent years, especially for enabling on-demand CPL switching. Electric field-induced control of CPL on/off switching is of particular interest because of its potential applications in optical information processing and advanced display technologies.[6–12]

Previously, our group demonstrated CPL on/off switching by doping an *N*-LC exhibiting positive dielectric anisotropy (*i.e.*, 4-cyano-4′-hexylbiphenyl (**6CB**)) with (*R*,*R*)/(*S*,*S*)-*N*,*N*′-bis(1-cyclohexylethyl)perylene-3,4,9,10-tetracarboxylic diimide ((*R*,*R*)/(***S*,*S***)-**CPDI**) as an emissive chiral dopant. In this system, the application of an electric field induced a phase transition from the chiral nematic phase to the nematic phase by eliminating the helical structure (Fig. 1).[13] This approach effectively enabled CPL switching *via* a phase transition mechanism. Additionally, by controlling the temperature, CPL modulation was achieved by utilising the phase transition between the LC phase and the isotropic liquid state.

In contrast to these previous approaches, the present study aims to successfully control the CPL by manipulating the orientation of the helical axis in the chiral nematic phase, while maintaining the helical structure itself. Specifically, an *N*-LC exhibiting a negative dielectric anisotropy (*i.e.*, *N*-(4-methoxybenzylidene)-4-butylaniline (**MBBA**)) is doped with an emissive chiral dopant to achieve dynamic and reversible CPL off/on switching by reorienting the helical axis under an applied electric field (Fig. 1). *N*-LCs with negative dielectric anisotropy are known to enable facile control of the molecular alignment under an applied electric field, contributing to stabilisation of the helical structure, which is advantageous for enhancing the CPL properties. Thus, in contrast to ***N**-LC-6CB/CPDI**, which allows for fast, reversible, and continuous on/off switching of the CPL intensity under an external electric field, this work aims to realise an ***N**-LC-MBBA/CPDI** system capable of off/on/off switching of the CPL intensity. Such an approach should open new pathways for the design of fast-response, robust CPL-active materials with high switching stabilities, which are crucial for the development of next-generation photonic devices.

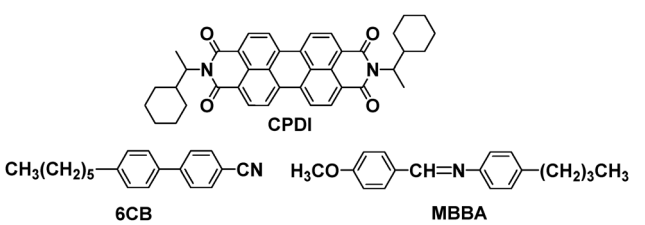

Fig. 1 Chiral perylene diimide luminophore **CPDI**, *N*-LC **6CB** exhibiting a positive dielectric anisotropy, and *N*-LC **MBBA** exhibiting a negative dielectric anisotropy.

[a] *Graduate School of Science and Engineering Kindai University, 3-4-1 Kowakae Higashi-Osaka, Osaka 577-8502, Japan. E-mail: y-imai@apch.kindai.ac.jp*
[b] *College of Liberal Arts and Sciences, Kitasato University, 1-15-1 Kitasato, Sagamihara, Kanagawa, 228-8555, Japan*

Fig. 2 POM image of ***N**-LC-MBBA/(*S*,*S*)-CPDI**.

The chiral emissive molecules, namely **(*R*,*R*)-CPDI** and **(*S*,*S*)-CPDI**, were synthesised according to previously reported procedures.[13] Subsequently, **(*R*,*R*)-** and **(*S*,*S*)-CPDI** were individually doped into the *N*-LC **MBBA** at a concentration of 1.0×10^{-2} M to prepare the target ***N**-LC-MBBA/(*R*,*R*)-CPDI** and ***N**-LC-MBBA/(*S*,*S*)-CPDI** systems, respectively. The resulting *N**-LC materials were encapsulated in conductive indium tin oxide glass cells to fabricate the LC devices.

The polarising optical microscopy (POM) image of ***N**-LC-MBBA/(*S*,*S*)-CPDI** obtained at 25 °C is shown in Fig. 2. A fingerprint texture characteristic of the chiral nematic (*N**) phase is clearly observed, indicating that **(*S*,*S*)-CPDI** effectively induces a pronounced helical arrangement (*i.e.*, chirality) in **MBBA**. This texture further suggests that the helical axis is aligned parallel to the cell substrate.

Subsequently, the chiroptical properties of ***N**-LC-MBBA/CPDI** were evaluated (Fig. 3). As previously reported, ***N**-LC-6CB/(R,R)-** and/**(*S*,*S*)-CPDI**, both of which exhibit positive dielectric anisotropy, demonstrate strong photoluminescence (PL) and CPL at an applied voltage of 0 V.[13] In contrast, in the ***N**-LC-MBBA/(R,R)-** and/**(*S*,*S*)-CPDI** systems, which exhibit negative dielectric anisotropy, PL was observed at 0 V, but CPL was not detected (Fig. 3a).

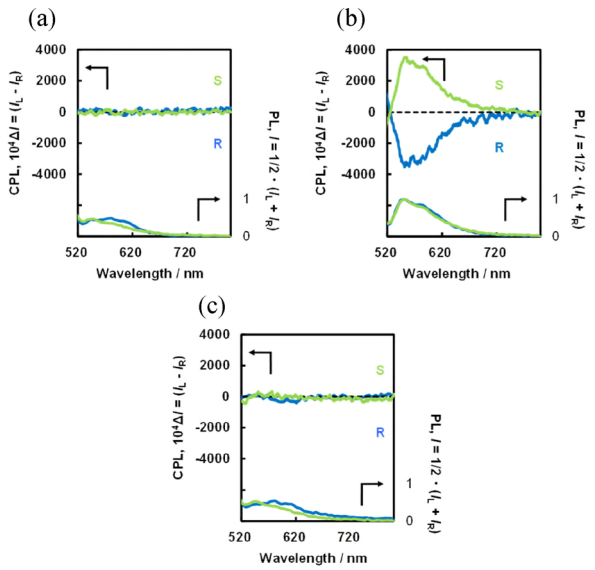

Fig. 3 CPL (top) and PL spectra (bottom) of ***N**-LC-MBBA/(*R*,*R*)-CPDI** (blue) and ***N**-LC-MBBA/(*S*,*S*)-CPDI** (green) along with their corresponding luminescence images (right-hand panels) acquired before voltage application (a) at 0 V, (b) at 5 V, and (c) after voltage application at 0 V. CPL and PL were performed at an excitation wavelength of 480 nm.

The observed emission wavelength (λ_{em}) of ***N**-LC-MBBA/CPDI** was approximately 550 nm, which originates from the fluorescence property of **CPDI**. The absence of CPL could be attributed to the perpendicular alignment of the LC molecules with respect to the cell plane in ***N**-LC-MBBA/CPDI**. In this system, the axis of the induced helical structure is oriented horizontally (*i.e.*, in the plane of observation) relative to the cell substrate. Such an alignment renders CPL emission along the observation direction particularly difficult; indeed, almost no CPL was detected experimentally. This was further supported by the clear fingerprint texture observed in the POM image, which confirms both the formation of a helical structure and the orientation of the helical axis (Fig. 2).

To elucidate the helical sense (chirality) of ***N**-LC-MBBA/CPDI**, a contact experiment was performed using cholesteryl oleyl carbonate (COC), a standard left-handed (M-helical) cholesteric material (Fig. 4). ***N**-LC-MBBA/CPDI** and COC were separately drop-cast onto different areas of a microscope slide, and covered with a cover glass for observation. Upon contact between these two samples, a continuous LC texture was observed at the centre of the cell when ***N**-LC-MBBA/(*S*,*S*)-CPDI** was employed, indicating that the helical senses of both samples were identical (Fig. 4a).

In contrast, when ***N**-LC-MBBA/(*R*,*R*)-CPDI** was used, a discontinuous texture was identified at the cell centre, reflecting the opposite helical senses of the two samples (Fig. 4b). These results demonstrate that **(*S*,*S*)-CPDI** induces a left-handed helix, whereas **(*R*,*R*)-CPDI** induces a right-handed helix in the *N*-LC host. In other words, **CPDI** can transfer its chirality to the achiral *N*-LC matrix of **MBBA** to generate a chiral nematic (*N**) phase with a helical sense corresponding to its own absolute configuration.

Subsequently, modulation of the ***N**-LC-MBBA/CPDI** optical properties was investigated under an applied voltage. Interestingly, upon applying an external voltage of 5 V, the CPL intensity of ***N**-LC-MBBA/CPDI** increased dramatically, enabling the efficient extraction of a strong CPL signal (Fig. 3b). The CPL spectra of ***N**-LC-MBBA/(*R*,*R*)-CPDI** and ***N**-LC-MBBA/(*S*,*S*)-CPDI** exhibited almost mirror-image relationships, with the CPL emission wavelength (λ_{CPL}) being observed at 553 nm. The CPL spectra originated from the chiral S_1 excited state, wherein a strong negative CPL signal was detected for ***N**-LC-MBBA/(*R*,*R*)-CPDI**, while a positive signal was observed for ***N**-LC-MBBA/(*S*,*S*)-CPDI**. The degree of circular polarisation in the excited state is defined by the dissymmetry factor (g_{CPL}) according to the equation $g_{CPL} = \Delta I/I = 2(I_L - I_R)/(I_L + I_R)$, where I_L and I_R are the emission

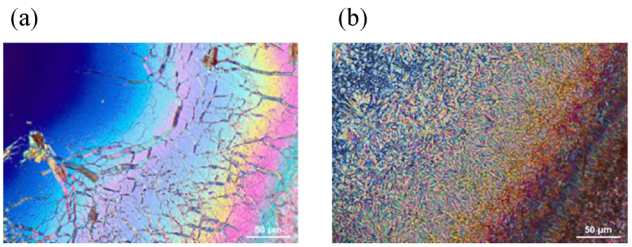

Fig. 4 POM images obtained for (a) ***N**-LC-MBBA/(*S*,*S*)-CPDI** and (b) ***N**-LC-MBBA/(*R*,*R*)-CPDI** in the contact experiment with COC.

intensities of left- and right-circularly polarised light, respectively, under non-polarised excitation. Consequently, the g_{CPL} value for ***N**-LC-MBBA/CPDI*** was determined to be approximately 0.36 at 553 nm. Given that the g_{CPL} value for the PMMA/CPDI film was previously reported to be 7.7×10^{-3}, the g_{CPL} for ***N**-LC-MBBA/CPDI*** is approximately 100-fold higher.[12] This significant enhancement can be attributed to the chiral **CPDI** molecules being effectively fixed within a suitably chiral environment formed by the surrounding **MBBA** LC molecules. Specifically, the molecular structure of **MBBA** is considered to form more specific and stronger interactions with the side chains of **CPDI**. As a result, chirality was more efficiently transferred from the chiral **CPDI** to the achiral **MBBA** LC, thereby leading to the formation of an effective chiral helical structure, which likely contributed to the high *g*-value. Additionally, the suppression of thermally induced non-radiative relaxation modes for **CPDI** and the selective reflection effect of ***N**-LC-MBBA** also likely contribute to the exceptionally high g_{CPL} value.

The POM image recorded for ***N**-LC-MBBA/CPDI** under an applied external electric field of 5 V is shown in Fig. 5(a). Under these conditions, a pronounced change in texture was observed, indicating dynamic reorientation of the helical axis in response to the applied field. Prior to the application of this direct current (DC) electric field, the LC molecules were aligned perpendicular to the substrate, with the helical axis oriented parallel to the substrate plane (*i.e.*, in-plane), resulting in a fingerprint texture. In contrast, upon application of the 5 V electric field, the LC molecules reoriented parallel to the substrate, accompanied by a reorientation of the helical axis perpendicular to the substrate plane (*i.e.*, out-of-plane). This reorientation led to a change in the POM image from the characteristic fingerprint texture to a dim twisted appearance. Interestingly, despite the disappearance of the fingerprint texture, the other measurements confirmed that the helical twisted structure was retained. This indicated that an applied electric field caused the rod-like LC molecules to align parallel to the substrate, whereas the helical axis was reoriented from a parallel to a perpendicular alignment with respect to the substrate surface. CPL measurements under an applied electric field showed an enhanced CPL intensity compared to the zero-field condition. This increase supports the conclusion that the helical twist structure was preserved even when an electric field was applied. This alignment was attributed to the negative dielectric anisotropy of the MBBA LC molecules, which causes the helical axis to orient perpendicular to the substrate. The absence of a visible colour does not mean that selective reflection is absent; rather, it suggests that the selective reflection wavelength shifts outside the visible spectrum. Therefore, Bragg reflection still occurs at wavelengths beyond the detection range of both the microscope and the human eye.

These findings demonstrate that the difference in the dielectric anisotropy of achiral LCs determines whether the CPL response follows an on/off or off/on switching pattern. This unique alignment, in which the helical axis is oriented normal to the substrate but the chiral twist remains intact, allows for dynamic and reversible control of the CPL by switching the electric field on and off. Such electric-field-induced modulation of the CPL intensity and the degree of polarisation holds significant potential for applications in advanced optical devices.

This CPL switching behaviour of ***N**-LC-MBBA/CPDI** can be explained by considering the following molecular alignment control. In ***N**-LC-MBBA**, the **CPDI** molecules align along the rod-like **MBBA** LC molecules, and the perylene diimide cores are approximately parallel to one another. However, they exhibit a torsional arrangement, thereby forming a structure analogous to the helical architectures of *N**-LCs. When using a vertically aligned cell, the LC molecules are aligned perpendicular to the substrate surface, resulting in an induced helical axis oriented parallel to the substrate plane. In this alignment state, because the observation direction is parallel to the helical axis, no CPL emission is observed at 0 V. In contrast, upon the application of a DC electric field (5 V), the **MBBA** LC molecules possessing negative dielectric anisotropy realign within the substrate plane (horizontal direction), concurrently reorienting the helical axis perpendicular to the substrate plane. During this process, the **CPDI** molecules undergo realignment following **MBBA** reorientation, forming an ideal helical structure that is oriented orthogonally to the observation direction, resulting in pronounced CPL emission. This change in the molecular alignment was corroborated by the POM images acquired under an applied electric field (Fig. 2 and 5), in which a shift from a fingerprint texture to a more uniform image was observed.

Finally, chiroptical measurements were performed under repeated DC electric field cycling (off (0 V)/on (5 V)/off (0 V)) to evaluate the reversibility and repeatability of the CPL switching (Fig. 6). Consequently, ***N**-LC-MBBA/CPDI** exhibited reversible and continuous CPL switching, clearly demonstrating that the application of a DC electric field enables a continuous and

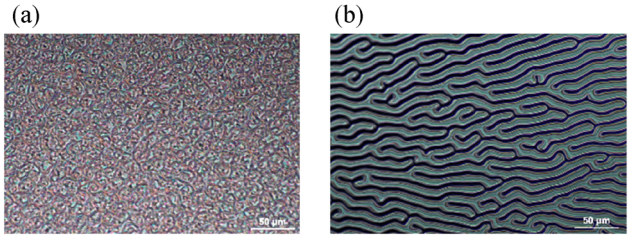

Fig. 5 POM images of ***N**-LC-MBBA/(*S*,*S*)-CPDI** acquired upon the application of a DC voltage at (a) 5 V and (b) the corresponding image after voltage application at 0 V.

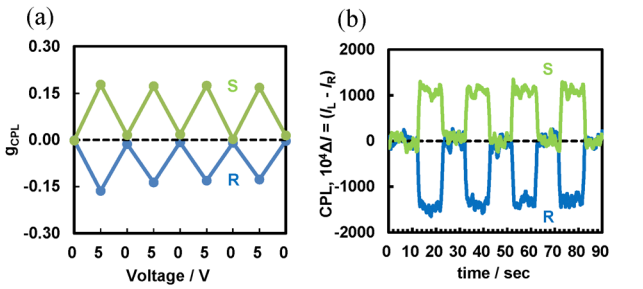

Fig. 6 (a) Switching g_{CPL} plots and (b) CPL intensity plots recorded for ***N**-LC-MBBA/(*R*,*R*)-CPDI** (blue) and ***N**-LC-MBBA/(*S*,*S*)-CPDI** (green) (553 nm CPL wavelength) under electric field cycling between 0 and 5 V.

reversible modulation of the CPL response. Notably, the response time was <1 s.

In this study, the dynamic and reversible control of CPL was demonstrated in a chiral *N**-LC system by manipulating the orientation of the helical axis under an applied electric field without disrupting the intrinsic helical structure. By doping an *N*-LC exhibiting negative dielectric anisotropy with an emissive chiral dopant, electric field-induced reorientation of the helical axis was achieved, *i.e.*, from a parallel to a perpendicular alignment relative to the substrate surface. Specifically, by combining the chiral perylene diimide-based emissive material **CPDI** with *N*-LCs possessing negative dielectric anisotropy (**MBBA**; yielding ***N**-LC-MBBA/CPDI**) or positive dielectric anisotropy (**6CB**; yielding ***N**-LC-6CB/CPDI**), completely opposite CPL switching behaviours were achieved under the application of a DC electric field. This approach offers a fundamentally different and potentially more stable method for CPL switching than phase transition-based techniques, thereby enabling efficient optical modulation. The ability to dynamically tune the CPL properties simply by controlling the helical axis orientation constitutes a significant step toward the use of such materials in advanced photonic applications.

Conflicts of interest

There are no conflicts to declare.

Data availability

The data supporting this article are included in the supplementary information (SI). Supplementary information is available. See DOI: **https://doi.org/10.1039/d5cp03335g**.

Acknowledgements

This work was supported by a JST-CREST grant (Grant Number JPMJCR2001), a Grant-in-Aid for Scientific Research (KAKENHI; Grant Numbers JP23H02040 and JP24K08087) from MEXT and JSPS, an IZUMI SCIENCE and TECHNOLOGY Foundation Research Grant (Grant Number 2024-J-062), and the Fujikura Foundation Research Grant (Grant Number 202514).

Notes and references

1 D. Zhao, F. Fan, J. Cheng, Y. Zhang, K. S. Wong, V. G. Chigrinov, H. S. Kwok, L. Guo and B. Z. Tang, *Adv. Opt. Mater.*, 2015, **3**, 199–202.
2 D. Y. Zhao, H. G. He, X. G. Gu, L. Guo, K. S. Wong, J. W. Y. Lam and B. Z. Tang, *Adv. Opt. Mater.*, 2016, **4**, 534–539.
3 Y. H. Shi, P. F. Duan, S. W. Huo, Y. G. Li and M. H. Liu, *Adv. Mater.*, 2018, **30**, e1705011.
4 X. J. Li, Q. Li, Y. X. Wang, Y. W. Quan, D. Z. Chen and Y. X. Cheng, *Chemistry*, 2018, **24**, 12607–12612.
5 Q. X. Jin, S. X. Chen, Y. T. Sang, H. Q. Guo, S. Z. Dong, J. L. Han, W. J. Chen, X. F. Yang, F. Li and P. F. Duan, *Chem. Commun.*, 2019, **55**, 6583–6586.
6 A. Bobrovsky, K. Mochalov, V. Oleinikov, A. Sukhanova, A. Prudnikau, M. Artemyev, V. Shibaev and I. Nabiev, *Adv. Mater.*, 2012, **24**, 6216–6222.
7 X. Li, Y. Shen, K. Liu, Y. Quan and Y. Cheng, *Mater. Chem. Front.*, 2020, **y**, 2954–2961.
8 L. Wang, A. M. Urbas and Q. Li, *Adv. Mater.*, 2020, **32**, e1801335.
9 X. Yang, M. Zhou, Y. Wang and P. Duan, *Adv. Mater.*, 2020, **32**, e2000820.
10 P. Lu, Y. Chen, Z. Chen, Y. Yuan and H. Zhang, *J. Mater. Chem. C*, 2021, **9**, 6589–6596.
11 K. Yao, Z. Liu, H. Li, D. Xu, W. H. Zheng, Y. W. Quan and Y. X. Cheng, *Sci. China: Chem.*, 2022, **65**, 1945–1952.
12 S. Suzuki, K. Kaneko, T. Hanasaki, M. Shizuma and Y. Imai, *ChemPhotoChem*, 2024, **8**, e202300224.
13 D. Suzuki, S. Suzuki, K. Kaneko, T. Hanasaki, M. Shizuma and Y. Imai, *Phys. Chem. Chem. Phys.*, 2025, **27**, 13519–13526.

